Analysis of tensile behavior of recycled aggregate concrete using acoustic emission technique

N. Williams Portal[1], M. Flansbjer[1], D. Carró-Lopez[2] and I. Fernandez[3]

[1] RISE Research Institutes of Sweden, Borås, Sweden
[2] Universidade da Coruña, La Coruña, Spain
[3] Chalmers University of Technology, Gothenburg, Sweden
natalie.williamsportal@ri.se

Abstract. Recycled concrete aggregate (RCA) was processed from reinforced concrete edge beams sourced from a demolished bridge. This material replaced different ratios of coarse aggregate in a benchmark concrete. The tensile behavior of the developed concrete mixes was characterized via monotonic and cyclic uni-axial tensile tests performed on notched cylinders. Such tensile tests allow for the quantification of the fracture energy and softening behavior of the concrete. Moreover, acoustic emission (AE) measurements were conducted in conjunction with the cyclic tests to characterize e.g. micro-crack initiation and development, as well as crack localization. The tensile behavior of the various materials was found to be similar with minimal variation in the results. However, the softening behavior suggests that the RCA materials are slightly more brittle compared to both the mother and benchmark materials. The corresponding AE measurements also indicated similarities between the micro-crack initiation and development for these mixes. It can be constituted that if the concrete used to produce RCA is of high quality and from one source, the resulting RAC will have adequate tensile properties with minimal variation, despite the aggregate replacement ratio.

Keywords: Recycled aggregates, Recycled aggregate concrete, Acoustic emission, Tensile behavior.

1 Introduction

1.1 Background

Closed-loop thinking is paramount concerning the responsible use of concrete as a building material. Residual concrete or demolition concrete waste can be crushed and recycled as aggregates and applied in new concrete or as filler material; the result of this being denoted as Recycled Concrete Aggregates (RCA). A promising market has been identified for re-use aggregates stemming from construction and demolition waste (CDW) in e.g. roads, drainage and other construction projects, but it is projected that the application can also be extended to structural applications.

1.2 Material source

The recycled material used in this work, funded by Infrasweden 2030: a strategic innovation program, was obtained from crushing edge beams from a demolished bridge in Gullspång, Sweden. The bridge was originally built in 1935, and due to heavy corrosion damages, it was demolished in 2016. It was presumed that the concrete had a remaining compressive strength of 30 MPa and smooth reinforcement bars with end hooks, which are typical for the given construction period.

1.3 Concrete recycling

Edge beams from the demolished bridge were processed with a transportable jaw-crusher that produced a recycled aggregate with coarse and fine fractions. A magnetic separator was attached to the crusher to recover most of the reinforcement for recycling. The processed material offered a continuous grain size distribution and it was divided into conventional sand (0/4 mm) and gravel fractions (8/16 and 16/25 mm). A low percentage of the crushed material was >25 mm which could undergo further crushing to yield smaller fractions. Only the coarse fraction (>4 mm) of this recycled aggregate was applied, which is the recommended in relevant EU regulations [1].

1.4 Recycled aggregate concrete

The effect of recycled aggregates in concrete with 0 %, 20%, 50% and 100 % of coarse recycled aggregates was analyzed. The concrete composition also included natural granitic sand (0/4 mm) and gravel (4/16 mm) as base materials. The cement used was a CEM I 42.5 R, which is very common in Swedish practice. To achieve acceptable workability a naphtalenesulfonate additive was used.

The reference concrete mixture applied can be found in [2]. The quantity of cement was 365 kg per cubic meter which is acceptable for aggressive environments. The w/c ratio was of 0.47 and was kept constant for all the coarse aggregate replacement (0%, 20%, 50%, 100%). The procedure to calculate the different mixes was to substitute the volume of the gravel with recycled gravel.

2 Uniaxial tensile tests

2.1 Test description

The tensile behavior of the concrete materials was obtained using uniaxial tensile tests (UTT). Such tensile tests allow for the quantification of the tensile strength, fracture energy and softening behavior of the concrete. Testing was performed on notched cylinder specimens with fixed end conditions following the recommendations given by RILEM [3] and [4]. In addition to monotonic tensile tests, cyclic tensile tests were performed on specimens of the RCA and benchmark materials.

As per Fig. 1, the tensile fracture process of concrete can be subdivided into four stages as defined in [5]; (I) elastic stage and (II) stable micro cracking in the pre-peak regime, and (III) unstable macro cracking and (IV) bridging in the post-peak regime,

i.e. softening behavior. The transitions between the different phases are however generally ambiguous and the phases are found to overlap. The fracture energy is defined as the energy needed to create one-unit of crack area, corresponding to the area under the softening curve, i.e. stress-crack opening relation.

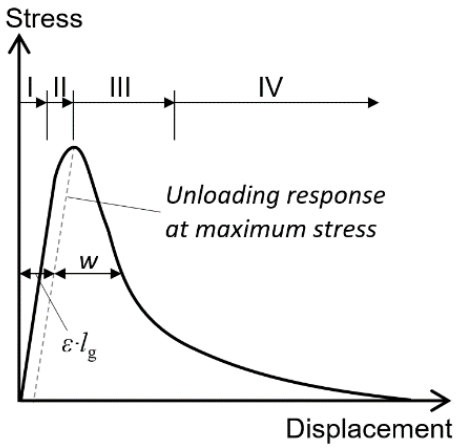

Fig. 1. Schematic representation of different phases of the cracking process in a typical stress-displacement relationship.

2.2 Test specimens and preparation

For the RAC and the benchmark materials, the specimens were manufactured from cast cylinders, while the specimens of the mother concrete were manufactured from cores taken from the edge beams. The top and bottom faces of the cylinders were face-ground to the final length to achieve plane parallel surfaces. The cylinder specimens had a final length of approximately 100 mm and a diameter of 100 mm. At the mid-section of the cylinders, a 10 mm deep and 5 mm wide circumferential notch was cut with a diamond blade (see Fig. 2). The diameter across the notch was measured at three separate locations along the perimeter; the average was used to calculate the cross-sectional area at the notch.

Each specimen was glued to a lower loading plate using a "glue device" to ensure that the center lines of the plate and specimen coincided, and perpendicularity between the face of the loading plate and the center axis of the specimen. The lower load plate, together with the glued-on specimen, was then bolted to the machine. Finally, the upper load plate, which was already attached to the machine, was glued to the top of the specimen. Hence, any small deviation from parallelism between the end faces of the specimen and the load plates are accommodated by the adhesive layers, yielding a perfect fit between the specimen and the load plates. The maximum difference in adhesive thickness over the area was approximately 0.1 mm, i.e. deviation from the specimen end faces being parallel. The adhesive used was X60 by HBM. The adhesive set for at least 30 minutes before testing to ensure sufficient strength.

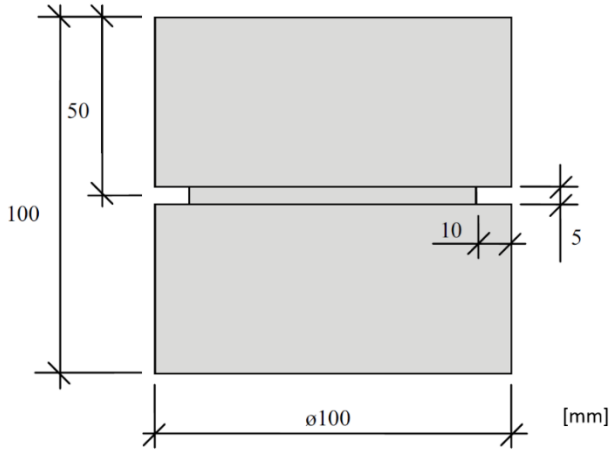

Fig. 2. Uniaxial tensile test specimen geometry.

2.3 Test setup and performance

The tests were displacement controlled and carried out in a GCTS servo-hydraulic machine with a high-stiffness load frame. The tests were conducted using a moment stiff loading device to suppress rotations of the load plates that could lead to bending failure. The device was pre-tensioned with a load of 150 kN. The load cell used was rated up to 200 kN and the accuracy of the load measurement was within 1%. The displacement was measured locally over the notch with three inductive displacement transducers with a gauge length, l_g, of 31 mm. The transducers had a measuring range of ±2.50 mm and a relative error of less than 1%. The gauges were approximately centered over the location of the notch. A photo of the of the test setup is shown in Fig. 3a.

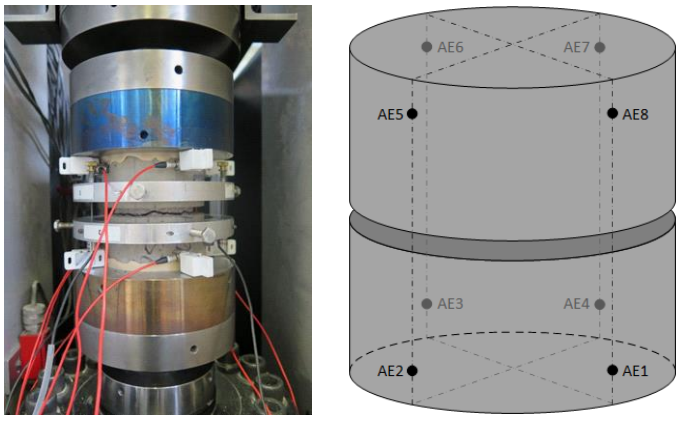

Fig. 3. Uniaxial tensile test setup with AE sensors during cyclic testing (a) and schematic of AE sensor locations and numbering on the specimen (b).

The average value of the three displacement transducers was used for the displacement control. In the monotonic tensile loading tests, the displacement was applied at a rate of 0.005 mm/min up to a displacement of $\delta = 0.05$ mm, 0.02 mm/min in the range $0.05 < \delta \leq 0.1$ mm, and then increased to 0.1 mm/min for the remaining part of the test until 0.5 mm was reached.

In the cyclic tensile loading test, four crack closing sequences were performed during the post-peak regime according to the schematic representation shown in Fig. 4; the peak being the tensile strength f_{ct}. During crack opening, the displacement rate was 0.005 mm/min up to $\delta = 0.1$ mm, 0.1 mm/min in the range $0.1 < \delta \leq 0.5$ mm, and then increased to 0.3 mm/min for the remaining part of the test until complete fracture was achieved, i.e. total separation of the two crack surfaces. The stress levels indicating the start of the crack closing sequences in Fig. 4 were chosen as $\sigma_1 = 2.6$, $\sigma_2 = 2.0$, $\sigma_3 = 1.4$ and $\sigma_4 = 0.8$ MPa. During the crack closing sequences, the displacement rate was -0.005 mm/min. When the compressive stress of $\sigma_{min} = 1$ MPa was reached, the loading was reversed to crack opening.

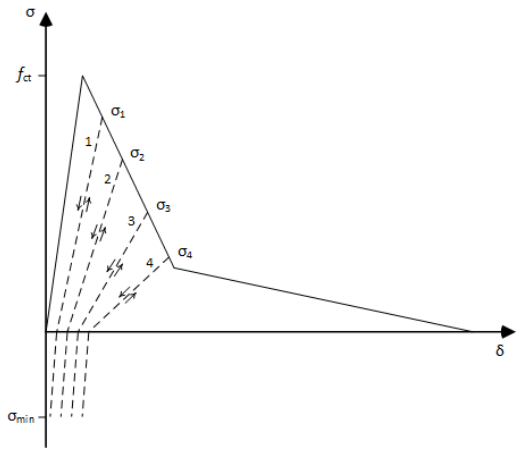

Fig. 4. Schematic representation of the cyclic loading sequences.

The crack opening w, in the post-peak regime, was evaluated according to [3] by subtracting the elastic deformation δ_e from the measured displacement δ as per Eq. (1):

$$w = \delta - \delta_e = \delta - (\sigma/E)\, l_g = \delta - \sigma/K \tag{1}$$

where σ is the tensile stress, E is the modulus of elasticity and l_g is the gauge length. Since the notch hampers the direct measurement of the modulus of elasticity in tension, the ratio E/l_g was replaced by the elastic stiffness K, which was evaluated directly from the tensile stress-displacement relationship as the secant modulus between origin and $0.45f_{ct}$. The fracture energy, G_F, was calculated from the area under the stress-crack opening curve as per Eq. (2):

$$G_F = \int \sigma(w)\, dw \tag{2}$$

2.4 AE measurements

An eight-channel Micro-II Digital AE system by Physical Acoustics Corporation was used for measuring and analyzing of AE. The AE activity was monitored by a total of eight AE sensors (Micro-30S) during tensile testing, four sensors placed close to each end face according to Fig. 3b. A pre-amplification of 40 dB and a threshold level of 50 dB were used. The hit detection parameters were set to PDT = 100 μs, HDT = 200 μs and HLT = 200 μs for all tests. At the time of each registered AE event, the load, actuator displacement and displacement of the three transducers were also recorded in the AE system. In addition to the parametric AE evaluation, the waveform of every hit was recorded and stored for all channels with a sample rate of 1 MSPS.

3 Experimental results

3.1 Monotonic tensile tests

The five different concrete materials described in Sections 1.2 and 1.4 were studied. The tensile behavior of the concrete, including the softening branch, was evaluated from uniaxial tensile tests performed on notched cylinder specimens with fixed end conditions as described in Section 2. The tensile stress-displacement relationships are shown in Fig. 5 for the mother concrete and Fig. 6 for benchmark, 20%, 50% and 100%. The tensile strength, f_{ct}, and the fracture energy, G_F, are summarized in Table 1.

Table 1. Monotonic tensile test result summary.

Concrete	Specimen ID	f_{ct} [MPa]	Avg (st dev.)	G_F [Nm/m^2]	Avg (st dev.)
Mother concrete	MC-1	2.9		232	
	MC-2	2.4		230	
	MC-3	2.6		153	
	MC-4	3.8	2.9 (0.5)	306	230 (54)
Benchmark	RT-1	3.0		157	
	RT-3	3.4		157	
	RT-4	3.4	3.3 (0.2)	212	175 (26)
20%	R20T-1	3.9		132	
	R20T-2	4.2		136	
	R20T-3	4.1	4.1 (0.1)	126	131 (4)
50%	R50T-1	3.1		131	
	R50T-2	3.2		105	
	R50T-3	3.7	3.3 (0.3)	137	124 (14)
100%	R100T-1	3.1		146	
	R100T-2	3.1		145	
	R100T-3	3.2	3.1 (0.1)	155	149 (5)

It can be noted that there is no major difference in the tensile behavior between the tested materials with respect to both strength and softening behavior. For all specimens, a non-linear stage of varying degree can be observed in the stress-displacement relation before peak stress, which is related to micro-cracking. Hence, there is no obvious difference in performance between the specimens with differing amounts of RCA replacement and the RCA materials also seem comparable to the benchmark material. However, the somewhat steeper softening curve that can be observed and the lower fracture energy suggest that the RCA materials are a bit more brittle compared to both the benchmark and mother materials.

In general, there is a larger scatter in both the tensile strength and fracture energy for the specimens from the mother material compared to the RCA and benchmark materials. For instance, specimen MC-4 exhibits noticeably higher tensile strength and fracture energy compared to the other specimens of the mother material. The higher fracture energy and the larger scatter is a consequence of the larger aggregates contained in the mother material, which especially affects the aggregate bridging taking place during the tail of the softening. Hence, the size and position of the larger aggregates in relation to the ligament area may have a significant influence on the fracture energy. Furthermore, since the cores were taken from different locations of the edge beam, material variations could be caused by differing batches.

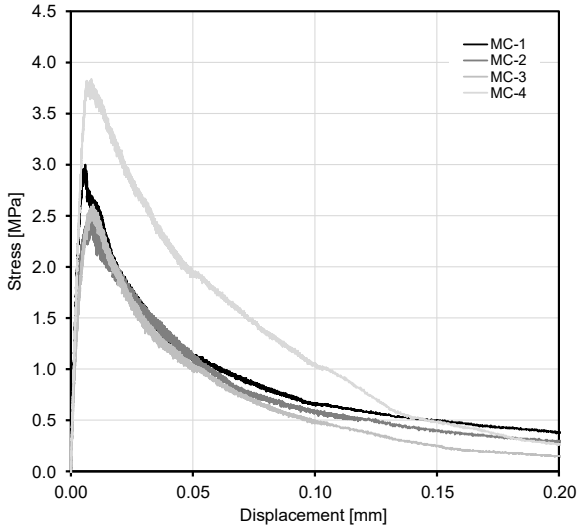

Fig. 5. Stress-displacement relations for the mother concrete (MC) specimens.

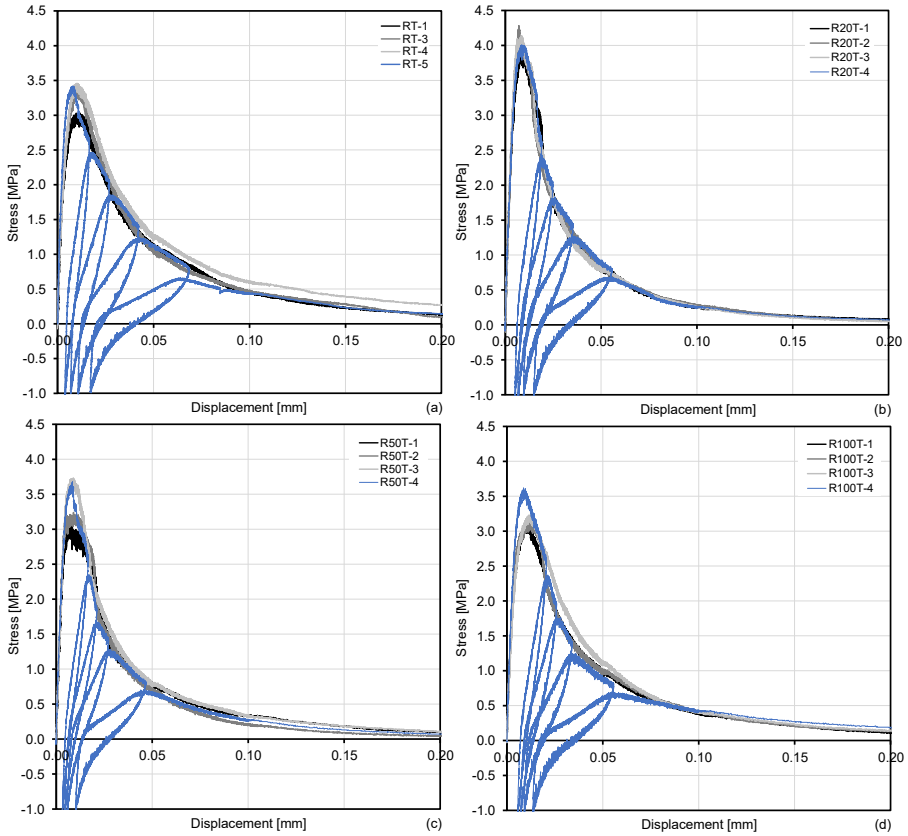

Fig. 6. Stress-displacement relations for RT (a), R20T (b), R50T (c) and R100T (d). Cyclic test results are presented for RT-5, R20T-4, R50T-4 and R100T-4.

3.2 Cyclic tensile tests

Cyclic tensile tests were performed on one specimen of each RCA material and the benchmark material. The stress-displacement relationships from the four tests are shown in Fig. 6a-d and compared with the monotonic tensile tests.

Comparing the stress displacement relations, it can be concluded that the overall behavior of the cyclic tensile tests is very similar to the monotonic tensile tests. Further, it can be observed that some irreversible deformation takes place during the crack closing cycles. Also, the hysteresis effect becomes larger with each cycle. The change in slope is notable during the closing phase going from tensile to compressive loading of the fracture zone. Similar observations can be noted during the crack opening phases. As expected, the increased damage in the fracture zone results in a successively decreased stiffness in the crack opening phase for each cycle.

Fig. 7 presents the development of AE activity (hits), crack opening and stress with respect to time. For clarity, the time is limited to the first 4000 s. The macro crack

initiation that is assumed to take place at peak stress is marked with a dashed line, while the crack closing phases are highlighted as grey zones.

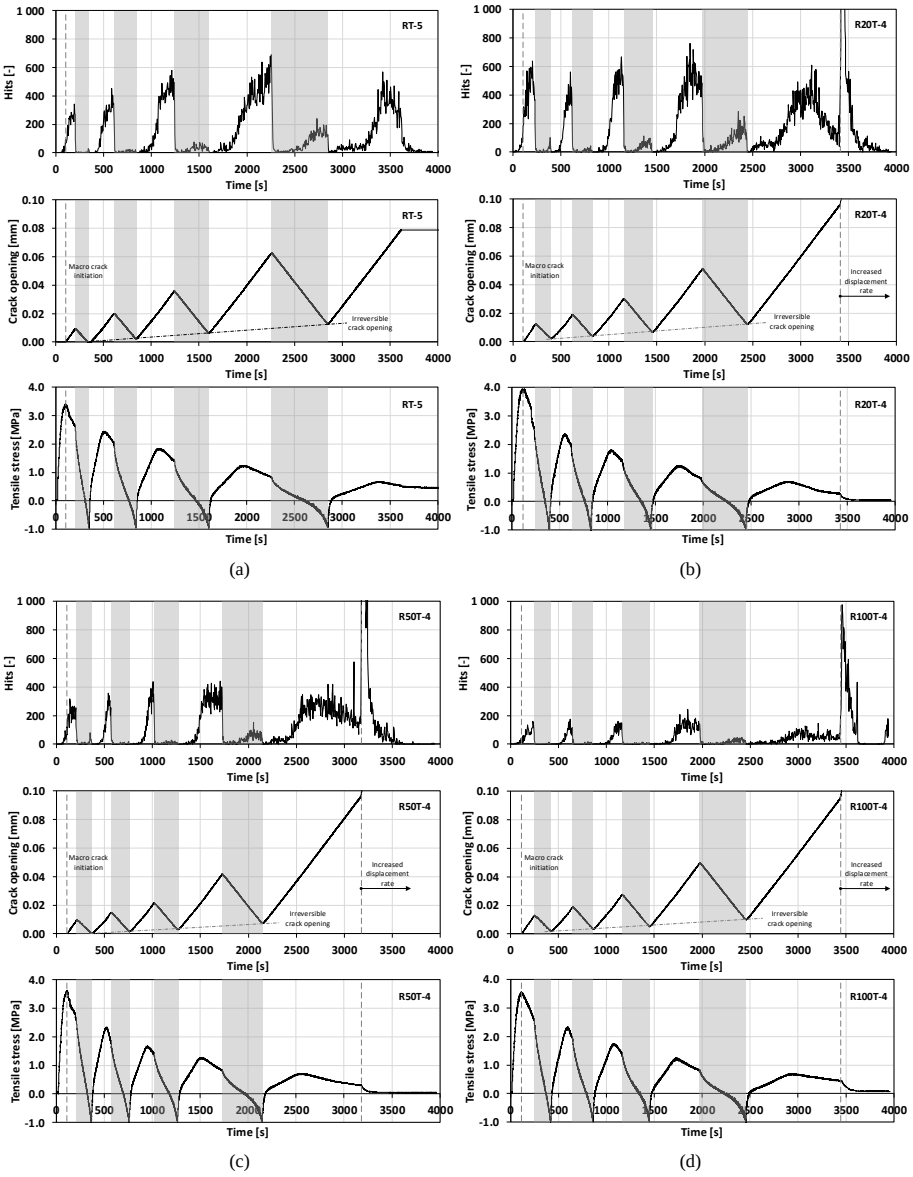

Fig. 7. Cyclic tensile test results summarized as Hit-time relation (upper), Crack opening-time relation (middle) and Stress-time relation (lower) for RT-5 (a), R20T-4 (b), R50T-4 (c) and R100T-4 (d).

The AE activity is zero during the first elastic stage in the pre-peak regime but increases during the second stage associated with micro-crack initiation taking place shortly before peak stress. The AE activity increases rapidly at the macro-crack initiation around peak stress. The relation between stress and AE activity (cumulative hits) during the initial fracture process with micro and macro-crack initiation is presented in more detail in Fig. 8 for the tested specimens, namely RT-5, R20T-4, R50T-4 and R100T-4.

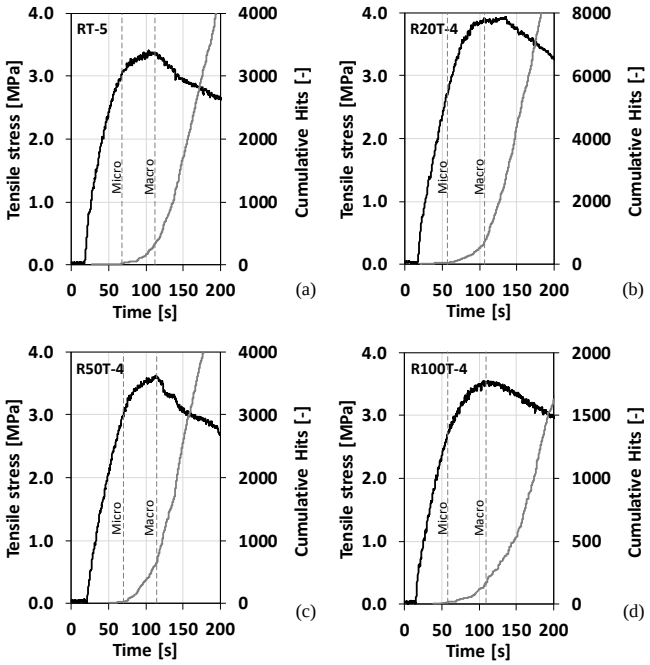

Fig. 8. Stress (black line) and cumulative hits (grey line) versus time for RT-5 (a), R20T-4 (b), R50T-4 (c) and R100T-4 (d). The approximate initiation of micro- and macro-cracking are indicated by dashed lines.

There is a clear reduction in AE activity as soon as the crack closing cycle starts, and the tensile stress is unloaded (see Fig. 7). The activity is much lower during the closing phases compared to the opening phases, although the activity increases somewhat when the fracture zone becomes subjected to compressive stress. In the subsequent crack opening phases, the AE activity initially decreases, but increases again significantly at a crack opening smaller than the maximum crack opening that was achieved during the former cycle, i.e. crack opening at the start of the previous crack closing phase.

From the crack opening diagrams in Fig. 7, the irreversible crack opening increases for each crack closing cycle for all specimens. This is likely related to an increased amount of debris and mismatch in the fracture zone. Also, the stiffness during the closing phase becomes lower for each cycle, which seems logical if the amount of debris to compact successively increases. This effect is also clearly reflected in the AE measurements as an increase in AE activity for each closing cycle.

The overall characteristics of the AE activity are rather similar, but the amount of AE activity differs slightly between the specimens. When comparing the results from R20T-4, R50T-4 and R100T-4, there is a tendency that the amount of AE activity decreases with increased amount of RCA replacement. This observation might indicate a slight difference in the fracture process associated to the RCA.

Moreover, the displacement rate was increased at a displacement of 0.1 mm, which resulted in a direct increase of AE activity in the form of increased hit rate in the hits-time diagrams (see Fig. 7). For specimen RT-5, this change in displacement rate was slightly delayed due to a shorter unforeseen pause in the test procedure at a displacement around 0.08 mm. As such, this resulting increase in AE activity was not related to a specific change in the cracking process, but rather due to an intensified crack activity related to the increased loading rate.

AE activity can be registered during the entire softening branch, also for larger crack openings where the stress transfer between the fracture surfaces is very limited. During the last stage (IV) related to gradual opening of the macro-crack, the AE activity is mainly caused by the bridging effect of the aggregate particles.

A 3D localization algorithm was used to determine the approximate location of the AE events. A projection of the location of all events with an amplitude above 70 dB is shown in Fig. 9. Although, it is difficult to correlate the AE events with the geometry of the real cracks, events with higher amplitudes (> 70 dB) can be correlated to the location of the developing fracture zone at the notch. The lower amplitude events ($\leq$ 70 dB) are more scattered in the specimens. The lower amplitude signals are more sensitive to attenuation when they travel through the material and as such it becomes harder to define the exact arrival time at the sensors making them more difficult to localize.

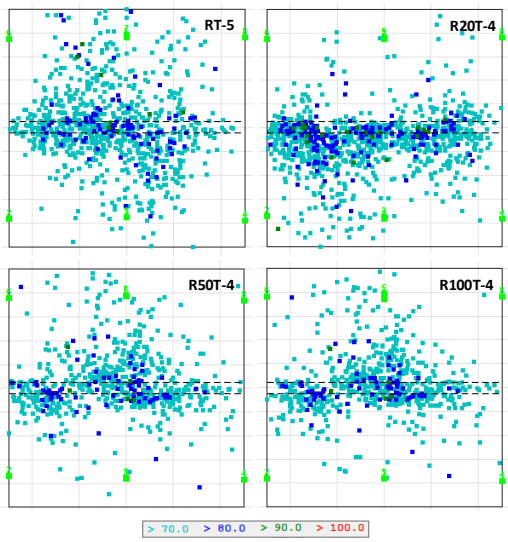

Fig. 9. Projection of the location of all events with an amplitude above 70 dB for RT-5, R20T-4, R50T-4 and R100T-4. The location of the notch is indicated by dashed lines and the position of AE sensors are indicated by light green squares.

4 Conclusions

Based on the conducted uniaxial tensile tests, no significant differences in the tensile behavior were noted between the specimens with different amounts of RCA replacement. The tensile behavior of the RCA materials was also comparable to the benchmark material. However, the observed softening behavior suggests that the RCA materials are slightly more brittle in comparison to both the mother and benchmark materials.

Furthermore, it was demonstrated that the AE activity measured during the cyclic tensile tests could be related to the different stages of the fracture process, associated with micro-crack initiation in the pre-peak regime, macro-crack initiation around peak stress, as well as the crack opening and crack closing cycles taking place during the post-peak regime. The AE activity also indicated similarities between the fracture process for the different mixes.

Another outcome of this work is related to the concrete source used to produce RCA. Making use of high-quality RCA from a unique source was shown to result in RAC with adequate tensile properties having minimal variation, regardless of the aggregate replacement ratio.

References

1. Tam, V.W.Y., Soomro, M., Evangelista, A.C.J.: A review of recycled aggregate in concrete applications (2000-2017). Constr. Build. Materi., 172, 272–292 (2018).
2. Carro-López, D., Fernandez, I., Williams Portal, N.: An old bridge transformed into a new one: Possible, recommendable? In: 20th IABSE Congress, New York City 2019: The Evolving Metropolis, pp. 951–956. International Association for Bridge and Structural Engineering (IABSE), Switzerland (2019).
3. RILEM TC 187-SOC: Experimental determination of the stress-crack opening: Final report. RILEM Publ. Bagneux (2007).
4. RILEM TC 162-TDF: Test and design methods for steel fibre reinforced concrete: Uni-axial tension test for steel fibre reinforced concrete. Materials and Structures, 34(235), 3–6 (2001).
5. van Mier, J.G.M.: Concrete Fracture, a Multiscale Approach. CRC Press, Boca Raton, Florida (2012).